# The Role of Thermal and Nonthermal Processes in Star Formation at the Galactic Center

F. Mazoochi *[1], F. Tabatabaei[1,2], C. Henkel[2], S. Longmore[3,4], and D. Walker[5]

[1]School of Astronomy, Institute for Research in Fundamental Sciences-IPM, Tehran, Iran
[2]Max-Planck-Institut für Radioastronomie, Auf dem Hügel 69, D-53121 Bonn, Germany
[3]Astrophysics Research Institute, Liverpool John Moores University, IC2, Liverpool Science Park, 146 Brownlow Hill, Liverpool L3 5RF, UK
[4]Cosmic Origins Of Life (COOL) Research DAO, https://coolresearch.io
[5]UK ALMA Regional Centre Node, Jodrell Bank Centre for Astrophysics, Oxford Road, The University of Manchester, Manchester M13 9PL, UK

**Abstract**

Centers of galaxies hosting supermassive black holes (SMBHs) drive extreme astrophysical processes that shape galaxy evolution. The circumnuclear region of the Galactic Center (GC) provides a unique laboratory to study these effects around Sgr A$^\star$. Using MeerKAT 1.3 GHz continuum and ALMA H40$\alpha$ data, we separate thermal free–free and nonthermal synchrotron emission at 18″ (0.7 pc) resolution. The correlation between nonthermal radio and FIR emission reveals a balance between magnetic, cosmic ray, and gas pressures, with an equipartition magnetic field averaging 445±7 $\mu$G and increasing toward Sgr A$^\star$. We find that the nonthermal pressure imposed by turbulent gas almost balances that of the magnetic field/cosmic rays and is about two orders of magnitude larger than the thermal pressure. Mass-to-flux ratios suggest a generally subcritical state, implying that magnetic fields play a key role in stabilizing clouds against collapse.

***Keywords:*** *Galactic Center — ISM — Thermal and Nonthermal — Magnetic Field*

## 1. Introduction

The Galactic Center (GC) at the center of the Milky Way is a key region for star formation and serves as the galactic nucleus where resolved studies of the interstellar medium (ISM) can be carried out using commonly available instruments (Yusef-Zadeh et al., 2013). Star formation activity in the GC has been examined in numerous studies (Barnes et al., 2017, Henshaw et al., 2022). Despite the abundance of molecular gas in this central region, which serves as the fuel for star formation, the star formation efficiency (SFE) in the GC is lower than expected (Longmore et al., 2013). The strong magnetic field, tidal shear, and turbulence are likely key factors influencing or regulating star formation within the molecular clouds of the Central Molecular Zone (CMZ) at the GC (e.g., Lu et al., 2024, Pillai et al., 2015).

The circumnuclear region surrounding the Supermassive Black Hole (SMBH) is a particularly intriguing area that requires dedicated study. Within this region, the circumnuclear disk (CND) constitutes the largest and nearest molecular gas structure to Sgr A$^\star$, exhibiting a quasi-Keplerian rotation(Liu et al., 2012, Martín et al., 2012). The disk extends from an inner radius of roughly 1.5–2 pc and is unlikely to exceed an outer radius of 7 pc (Christopher et al., 2005, Genzel et al., 1985). The CND is distinguished by its strong magnetic field and supersonic motions (Akshaya & Hoang, 2024, Guerra et al., 2023). The neutral gas within the disk has densities of $\sim 10^5\,\mathrm{cm}^{-3}$, and its total hydrogen mass is estimated at $\sim 10^4\ M_\odot$ (Genzel et al., 1985, Mezger et al., 1996). Inside the innermost ∼2 pc of this region lies the mini-spiral structure (Sgr A West), where $A_v$ ranges from 20 to 50 mag (Scoville et al., 2003). While tidal shear hinders the onset of star formation near the SMBH, a massive stellar cluster is nevertheless observed within the central parsec, in close proximity to Sgr A$^\star$ (Schödel et al., 2009, Yusef-Zadeh et al., 2015). Probing the physical conditions of the ISM is therefore crucial for unraveling the mysteries of this central region.

Our study aims to clarify the roles of thermal and nonthermal processes in shaping the ISM of GC structure, examining the interconnections between ISM components and the impact of the SMBH on these

*famazoochi@ipm.ir, Corresponding author

relationships. To achieve this, we first separate the radio continuum (RC) emission into its two constituent parts: synchrotron (nonthermal) and free-free (thermal). The synchrotron component, produced by relativistic cosmic ray electrons (CREs) interacting with magnetic fields, follows a power-law spectrum ($S_\nu \propto \nu^{-\alpha_n}$). In contrast, the free-free component, emitted by thermally ionized gas, has a much flatter spectral index (approximately $-0.1$) under optically thin conditions ($\tau_\nu \ll 1$).

## 2. Data

In this study, we used a combination of the radio and IR observations of the circumnuclear region, which are outlined in Table 1 and explained in order of wavelength.

Table 1. Summary of data used in this study

| Data | Frequency/ Wavelength | Angular Resolution | Calibration noise | Telescope | Reference |
|---|---|---|---|---|---|
| RC | 1.3 GHz | $4'' \times 4''$ | 5% | MeerKAT | Heywood et al. (2022) |
| H40$\alpha$ | 99.0 GHz | $1.4'' \times 1.2''$ | 5% | ALMA | Hsieh et al. in prep |
| CO J=1→0 | 115.3 GHz | $15'' \times 15''$ | 6.4% | NRO | Tokuyama et al. (2019) |
| CO J=3→2 | 345.8 GHz | $15'' \times 15''$ | 6% | JCMT | Eden et al. (2020) |
| FIR | 160 $\mu$m | $12'' \times 12''$ | 5% | Herschel | Molinari et al. (2010) |
| FIR | 70 $\mu$m | $6'' \times 6''$ | 5% | Herschel | Molinari et al. (2010) |
| MIR | 21.3 $\mu m$ | $18.3'' \times 18.3''$ | 6% | SPIRIT III | Price et al. (2001) |

All data in this study were convolved to the worst resolution of $18.3'' \times 18.3''$ in the Astronomical Image Processing System (AIPS) software by using an elliptical Gaussian kernel. The total uncertainty ($\sigma$) in the observed intensities incorporates both statistical errors (the map's root mean square noise, $\sigma_{\rm rms}$) and systematic errors (the instrumental flux calibration uncertainty, $\sigma_{\rm cal}$). We calculate this total uncertainty for each data point using the formula $\sigma = \sqrt{(\sigma_{\rm cal} \times F_\nu)^2 + \sigma_{\rm rms}^2}$, where $F_\nu$ is the flux density. Errors in the final parameters derived in this study are determined by propagating these $\sigma$ uncertainties through the reported measurements.

## 3. Analysis

### 3.1. Separation of Thermal and Nonthermal Emission

In this section, we derive maps for the thermal and nonthermal components of the 1.3 GHz of RC emission within the circumnuclear region using the Thermal Radio Tracer (TRT) method (Tabatabaei et al., 2007). Because this region suffers from high extinction, the standard H$\alpha$ recombination line is unsuitable as a thermal tracer. Unlike H$\alpha$, radio recombination lines (RRLs) are not affected by dust extinction (Scoville et al., 2003), making them a more robust tracer for the free-free emission in this dusty environment. In the TRT method, to measure thermal emission under local thermal equilibrium (LTE), we first need to calculate the emission measure (EM) in optically thin conditions using the following relation:

$$\frac{T_L \Delta v}{K\,km\,s^{-1}} = 5.76 \times 10^2 \left(\frac{T_e}{K}\right)^{-1.5} \left(\frac{EM}{cm^{-6}\,pc}\right) \left(\frac{\nu_L}{GHz}\right)^{-1}. \quad (1)$$

In this formula, $T_L \Delta v$ is the integrated line intensity over the velocity width of the line (measured in units of $K.Km\,s^{-1}$), $\nu_L$ is the frequency of the RRL, and $T_e$ represents the electron temperature.

Conversely, we can derive the optical depth of the continuum emission at the frequency ($\nu_c$) directly from the Emission Measure (EM) using this formula:

$$\tau_c = 8.23 \times 10^{-2} \times \left(\frac{T_e}{K}\right)^{-1.35} \left(\frac{EM}{cm^{-6}pc}\right) \left(\frac{\nu_c}{GHz}\right)^{-2.1}. \quad (2)$$

The brightness temperature (flux density) of the radio continuum emission, $T_c$, is derived from the radiative transfer equation:

$$T_c^{th} = T_e(1 - e^{-\tau_c}). \quad (3)$$

In this study, we use the H40$\alpha$ recombination line ($\nu_L$ =99 GHz) from the ALMA CMZ Exploration Survey (ACES) as our thermal tracer to measure the EM. We adapted the average value of $T_e = 6000$ K in this region (Hsieh et al., 2018, Lang et al., 2001, Scoville et al., 2003).

In the end, we obtain the nonthermal flux density by subtracting the thermal emission flux density from the total continuum emission at the continuum frequency ($S_{\nu_c}^{nt} = S_{\nu_c}^{RC} - S_{\nu_c}^{nt}$). The resulting maps of the thermal and nonthermal emission are shown in Figure 1. The thermal fraction ($f_{\nu_c}^{th} = S_{\nu_c}^{th}/S_{\nu_c}^{RC}$) is generally highest ($f^{1.3} \simeq 30 - 39\%$) on a lane extended from the south of Sgr A$^\star$ to the east.

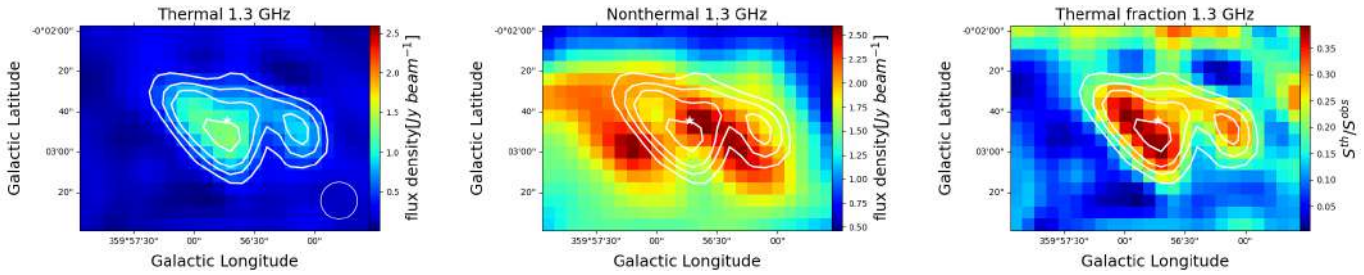


Figure 1. Map of the thermal (left), nonthermal (middle, superposed on the thermal contours) and thermal fraction (right) of the circumnuclear region at the frequency of 1.3 GHz in the resolution of 18".

## 3.2. Radio-IR Correlation

The Radio-IR correlation can unveil the interplay between massive star formation and magnetized/relativistic ISM when studied locally inside galaxies. As such, studying this correlation on resolved scales provides, in general, a useful tool to infer the propagation length of cosmic ray electrons and the mixing/coupling of magnetic field and gas (Tabatabaei et al., 2013). Figure 2 shows correlations between thermal (free) and nonthermal (synchrotron) emissions at 1.3 GHz with 160, 70, and 21 $\mu$m emissions in our study region. The strong correlations between nonthermal and IR emissions, as indicated by Pearson correlation coefficients ($R_p \geq 0.6$), suggest a fine balance between the cosmic ray electrons, magnetic fields, and gas pressure.

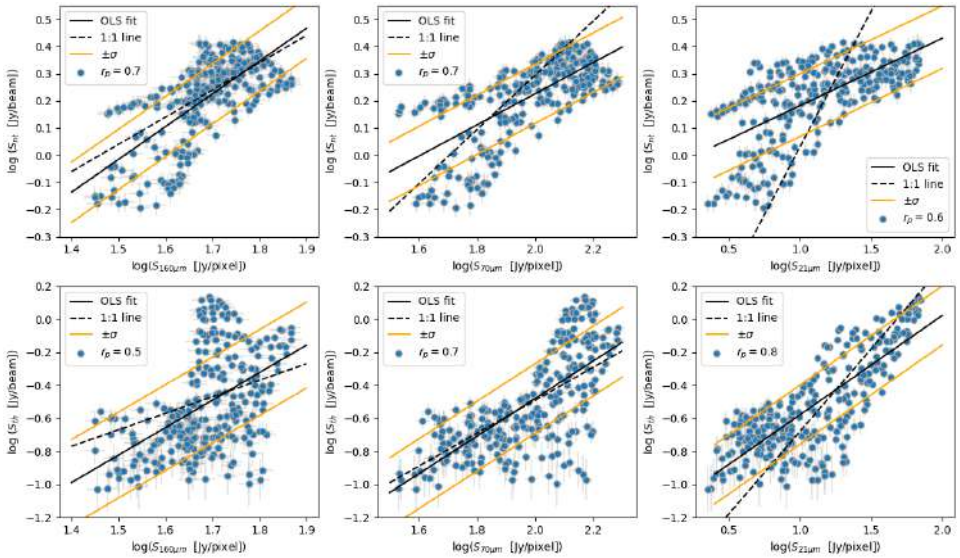


Figure 2. Correlations between the thermal ($S_{th}$, lower panels) and nonthermal ($S_{nt}$, upper panels) emission at 1.3 GHz with the 160, 70, and 21 $\mu$m IR emissions in the central region. The solid black line indicates the OLS fitting, the dashed line represents the 1:1 line, and the orange lines are 1 $\sigma$ scatter lines.

The solid black lines in Figure 2, show the ordinary least squares (OLS) fits to the data, and the dashed lines mark the 1:1 lines. When the solid lines are close to the 1:1 lines, it indicates a mostly linear scaling relation. The nonthermal–160 $\mu$m and thermal–70 $\mu$m correlations indicate such a linear relationship between these emissions.

### 3.3. Equipartition Magnetic Field

There are several approaches to estimate the magnetic field strength in galaxies. One commonly used method relies on synchrotron emission under the assumption that the energy density of cosmic rays is equal to that of the magnetic field (the B/CR equipartition), which has also been applied in Galactic Center studies using data and MHD models (e.g., LaRosa et al., 2004, Yusef-Zadeh et al., 2022, **?**). Under this equipartition condition, where the energy densities of cosmic rays and magnetic fields are equal ($\epsilon_{CR} = \epsilon_B = B_{eq}^2/8\pi$), the total magnetic field strength can be derived from the nonthermal (synchrotron) intensity, $I_n$, by replacing $n_e$ in the cosmic-ray energy density with the synchrotron intensity (Beck & Krause, 2005). The equipartition magnetic field is given by the following equation:

$$B_{eq} = C(\alpha_n, K, L) I_n^{1/(\alpha_n+3)} \tag{4}$$

where C is a function of the nonthermal spectral index ($\alpha_n$), the ratio between the number densities of cosmic ray protons and electrons (K), and the path length through the synchrotron emitting medium (L). By assuming $\alpha_n = 0.7$ (Sato et al., 2024), K=100 (Beck & Krause, 2005) and L=11 pc (Blank et al., 2016, Oka et al., 2011), we mapped the equipartition magnetic field in this region (see Figure 3-left).

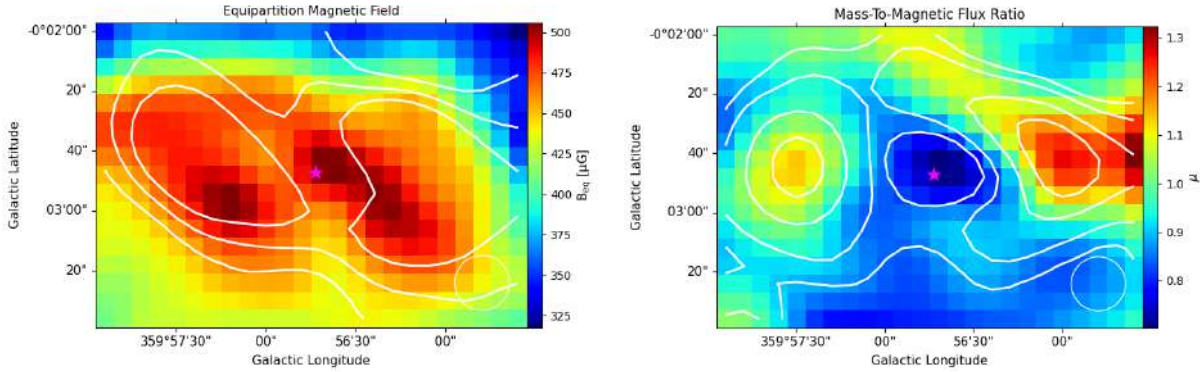


Figure 3. Maps of equipartition magnetic field (left) and mass-to-magnetic flux ratio (right) in the circumnuclear region at the resolution of 18".

## 4. Discussion

### 4.1. Energy Balance

Examining the energy balance of the ISM within the inner 7 pc of the SMBH is crucial for understanding its physical state. The total energy content of the ISM is governed by the kinetic energy of turbulent motions ($E_k = \frac{1}{2}\rho\sigma_v^2$), the thermal energy of various gas phases ($E_{th} = \frac{3}{2}nKT$), and the nonthermal contributions from magnetic fields and cosmic rays ($E_{nt} = 4E_b = B^2/4\pi$) (Tabatabaei et al., 2018). By accessing mass and number densities ($\rho$ and n), velocity dispersion ($\sigma_v$), and temperature (T) for different phases of the ISM, we can measure the thermal and kinetic energy densities. Based on the equipartition assumption and measuring $B_{eq}$ (see section 3.3), we obtain the nonthermal energy density in the circumnuclear region. The results of measuring these energy densities are indicated in the radial profiles in Figure 4. This figure demonstrates that the nonthermal and kinetic energy densities are considerably greater than the thermal energy density in this region, with the kinetic energy density being slightly higher than the nonthermal energy density.

### 4.2. Mass-to-Magnetic Flux ratio

A classical approach to investigating the impact of the magnetic field on gravitational collapse and star formation is measuring the ratio of the gas mass to the magnetic flux ($M/\Phi_B$) (Crutcher, 1999). We obtained the equipartition magnetic field strength ($B_{eq}$) and the molecular gas column density ($N(H_2)$) from the nonthermal intensity (see section 3.3), and the CO map intensity ($N(H_2) = X_{CO} \times I_{CO}$). From the following equation (Crutcher, 2012), we can measure this parameter in units of the critical value ($\mu_0 = (2\pi G)^{-1}$):

$$\mu = 7.6 \times 10^{-21} \frac{N(H_2)[cm^{-2}]}{B_{tot}[\mu G]} \tag{5}$$


doi:https://doi.org/10.52526/25792776-25.72.2-363

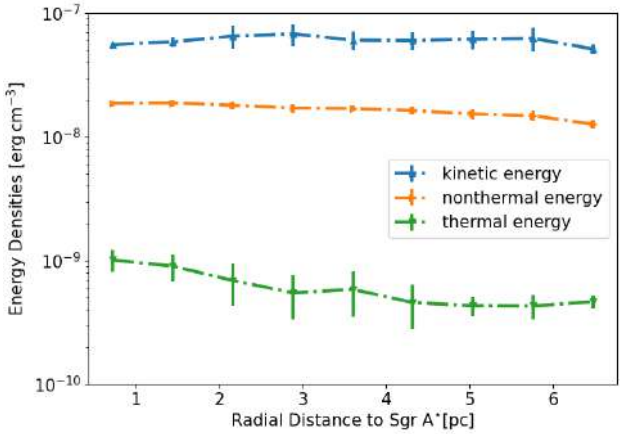


Figure 4. Radial profiles of energy densities in the circumnclear region.

In Figure 3-right, the map of $\mu$ is indicated. Molecular clouds are considered critical when $\mu = 1$, and subcritical when $\mu < 1$, in which case a strong magnetic field can inhibit gravitational collapse. Conversely, if $\mu > 1$, the clouds are regarded as supercritical, making them unstable to gravitational collapse, thereby allowing star formation to proceed (Crutcher, 1999). Taking more realistic conditions into account, Mouschovias (1991) derived a larger critical value of $\mu \simeq 2$. In this region, we find an average value of $\mu = 0.91 \pm 0.02$, indicating a subcritical condition.

## 5. Conclusion

To study the energy balance, structure formation, and physical condition in the ISM of the circumnuclear region, we separate the thermal and nonthermal components of RC emission at 1.3 GHz using the H40 RRL as an extinction-free tracer of the free-free emission by the thermal radio template (TRT) method. We found that within 7 pc distance from the Sgr A$^\star$, the nonthermal component dominates the thermal at 1.3 GHz frequency. In addition, the radio-IR correlations are investigated, indicating a fine balance between the cosmic ray electrons, magnetic fields, and gas pressure. Therefore, we applied the equipartition assumption to estimate the lower limit of the magnetic field strength. The derived mean value of $B_{eq}$ is $445 \pm 7\,\mu$G.

Through this study, the separation results and the equipartition assumption enable us to examine the role of the magnetic field on star formation in this region. We computed the energy content of the interstellar medium (ISM), which encompasses the thermal, nonthermal, and kinetic energy densities. This study discovered that the kinetic and nonthermal energy densities dominate the thermal energy density. Based on the computed mass-to-magnetic flux ratio ($\mu$) and the critical value ($\mu_{crit} \sim 1 - 2$), this region is classified as a subcritical region, indicating that the magnetic field can protect clumps of this region against the gravitational collapse.

In the end, we demonstrate that the ISM in this region exhibits significant complexity. With upcoming surveys and larger datasets, more existing open questions in the Galactic Center will be answered in the future.

**Acknowledgements**

We would like to thank Dr. Ashley Barnes, Dr. Laura Colzi, Dr. Pablo Garcıa, Dr. Yue Hu, Dr. Sergio Martın, Dr. Álvaro Sánchez-Monge, Dr. Vıctor M.Rivilla, Dr. Anika Schmiedeke, Dr. Juergen Ott, Dr. Daniel Wang, Dr. Gwenllian Williams, and Dr. Suinan Zhang for their precious and constructive comments, which greatly contributed to enhancing the quality of this paper.

## References

Akshaya M., Hoang T., 2024, Monthly Notices of the Royal Astronomical Society, p. stae1464

Barnes A., Longmore S., Battersby C., Bally J., Kruijssen J., Henshaw J., Walker D., 2017, Monthly Notices of the Royal Astronomical Society, 469, 2263

Beck R., Krause M., 2005, Astronomische Nachrichten: Astronomical Notes, 326, 414

Blank M., Morris M. R., Frank A., Carroll-Nellenback J. J., Duschl W. J., 2016, Monthly Notices of the Royal Astronomical Society, 459, 1721

Christopher M. H., Scoville N., Stolovy S., Yun M. S., 2005, The Astrophysical Journal, 622, 346

Crutcher R. M., 1999, The Astrophysical Journal, 520, 706

Crutcher R. M., 2012, Annual Review of Astronomy and Astrophysics, 50, 29

Eden D. J., et al., 2020, Mon. Not. R. Astron. Soc. , 498, 5936

Genzel R., Watson D. M., Crawford M., Townes C., 1985, Astrophysical Journal, Part 1 (ISSN 0004-637X), vol. 297, Oct. 15, 1985, p. 766-786., 297, 766

Guerra J. A., Lopez-Rodriguez E., Chuss D. T., Butterfield N. O., Schmelz J. T., 2023, The Astronomical Journal, 166, 37

Henshaw J. D., Barnes A. T., Battersby C., Ginsburg A., Sormani M. C., Walker D. L., 2022, arXiv preprint arXiv:2203.11223

Heywood I., et al., 2022, The Astrophysical Journal, 925, 165

Hsieh P.-Y., Koch P. M., Kim W.-T., Ho P. T., Tang Y.-W., Wang H.-H., 2018, The Astrophysical Journal, 862, 150

LaRosa T., Nord M. E., Joseph T., Lazio W., Kassim N. E., 2004, The Astrophysical Journal, 607, 302

Lang C. C., Goss W. M., Morris M., 2001, The Astronomical Journal, 121, 2681

Liu H. B., Hsieh P.-Y., Ho P. T., Su Y.-N., Wright M., Sun A.-L., Minh Y. C., 2012, The Astrophysical Journal, 756, 195

Longmore S., et al., 2013, Monthly Notices of the Royal Astronomical Society, 429, 987

Lu X., et al., 2024, The Astrophysical Journal, 962, 39

Martín S., Martín-Pintado J., Montero-Castaño M., Ho P., Blundell R., 2012, Astronomy & Astrophysics, 539, A29

Mezger P. G., Duschl W. J., Zylka R., 1996, The Astronomy and Astrophysics Review, 7, 289

Molinari S., et al., 2010, Publications of the Astronomical Society of the Pacific, 122, 314

Mouschovias T. C., 1991, Astrophysical Journal, Part 1 (ISSN 0004-637X), vol. 373, May 20, 1991, p. 169-186. NSF-supported research., 373, 169

Oka T., Nagai M., Kamegai K., Tanaka K., 2011, The Astrophysical Journal, 732, 120

Pillai T., Kauffmann J., Tan J. C., Goldsmith P. F., Carey S. J., Menten K. M., 2015, The Astrophysical Journal, 799, 74

Price S. D., Egan M. P., Carey S. J., Mizuno D. R., Kuchar T. A., 2001, The Astronomical Journal, 121, 2819

Sato K., Shinnaga H., Furuya R. S., Suzuki T. K., Kakiuchi K., Ott J., 2024, Publications of the Astronomical Society of Japan, 76, 960

Schödel R., Merritt D., Eckart A., 2009, Astronomy & Astrophysics, 502, 91

Scoville N., Stolovy S., Rieke M., Christopher M., Yusef-Zadeh F., 2003, The Astrophysical Journal, 594, 294

Tabatabaei F., Beck R., Krügel E., Krause M., Berkhuijsen E., Gordon K., Menten K., 2007, Astronomy & Astrophysics, 475, 133

Tabatabaei F. S., et al., 2013, Astron. Astrophys. , 552, A19

Tabatabaei F., Minguez P., Prieto M., Fernández-Ontiveros J., 2018, Nature Astronomy, 2, 83

Tokuyama S., Oka T., Takekawa S., Iwata Y., Tsujimoto S., Yamada M., Furusawa M., Nomura M., 2019, Publications of the Astronomical Society of Japan, 71, S19

Yusef-Zadeh F., et al., 2013, The Astrophysical Journal Letters, 767, L32

Yusef-Zadeh F., et al., 2015, The Astrophysical Journal, 808, 97

Yusef-Zadeh F., Arendt R., Wardle M., Heywood I., Cotton W., Camilo F., 2022, The Astrophysical Journal Letters, 925, L18